Refractive Index Sensing with Subradiant Modes: A Framework To Reduce Losses in Plasmonic Nanostructures

Benjamin Gallinet[†,‡,*] and Olivier J. F. Martin[‡]

[†]CSEM Muttenz, Tramstrasse 99, CH-4132 Muttenz, Switzerland and [‡]Nanophotonics and Metrology Laboratory, Swiss Federal Institute of Technology (EPFL), CH-1015 Lausanne, Switzerland

ABSTRACT Plasmonic modes with long radiative lifetimes, subradiant modes, combine strong confinement of the electromagnetic energy at the nanoscale with a steep spectral dispersion, which makes them promising for biochemical sensors or immunoassays. Subradiant modes have three decay channels: Ohmic losses, their extrinsic coupling to radiation, and possibly their intrinsic dipole moment. In this work, the performance of subradiant modes for refractive index sensing is studied with a general analytical and numerical approach. We introduce a model for the impact that has different decay channels of subradiant modes on the spectral resolution and contrast. It is shown analytically and verified numerically that there exists an optimal value of the mode coupling for which the spectral dispersion of the resonance line shape is maximal. The intrinsic width of subradiant modes determines the value of the dispersion maximum and depends on the penetration of the electric field in the metallic nanostructure. A figure of merit, given by the ratio of the sensitivity to the intrinsic width, which are both intrinsic properties of subradiant modes, is introduced. This figure of merit can be directly calculated from the line shape in the far-field optical spectrum and accounts for the fact that both the spectral resolution and contrast determine the limit of detection. An expression for the intrinsic width of a plasmonic mode is derived and calculated from the line shape parameters and using perturbation theory. The method of analysis introduced in this work is illustrated for dolmen and heptamer nanostructures. Fano-resonant systems have the potential to act as very efficient refractive index sensing platforms compared to Lorentz-resonant systems, due to control of their radiative losses. This study paves the way toward sensitive nanoscale biochemical sensors and immunoassays with a low limit of detection and, in general, any nano-optical device where Ohmic losses limit the performance.

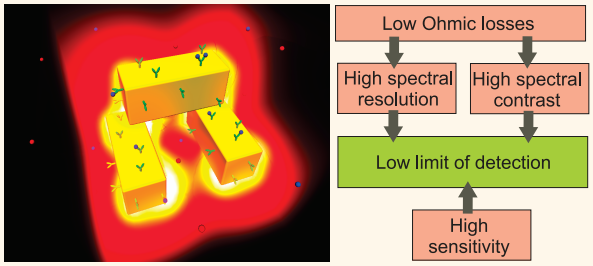

KEYWORDS: Fano resonances · electromagnetically induced transparency · plasmonic nanosensors · refractive index sensing · figure of merit · loss engineering

Surface plasmon resonances possess the ability to confine light at the nanoscale, below the diffraction limit.[1,2] They have attracted strong interest in the past decade in the context of biochemical sensing and immunoassays because a nanoscale perturbation of their local environment can be probed optically.[3−5] Their high sensitivity has been instrumental to push the detection limit of optical sensors toward a single molecule.[3−5] Such a real-time detection method also has the additional advantage of being label-free. It has been recently combined with nano-optical trapping and manipulation[6,7] and extended to other sensing concepts such as nanocalorimetry.[8] Compact plasmonic resonators also enable reaching a subcellular resolution, which has the potential to improve the understanding of subcellular processes.[5,9] From the optical point of view, a shift of the resonance frequency of a plasmonic resonator occurs when the dielectric properties of the local environment change upon binding of any analyte under study.[10] Both the sensitivity of the plasmonic mode and the uncertainty in the determination of its resonance frequency determine the detection limit.[11,12] Plasmonic modes with a long radiative lifetime, subradiant modes, possess a strong spectral dispersion which further improves the limit

* Address correspondence to benjamin.gallinet@csem.ch.

Received for review May 1, 2013 and accepted July 20, 2013.

Published online July 20, 2013
10.1021/nn4021967

of detection and makes them very attractive for sensing applications.[13,14] When subradiant modes are coupled to radiation or to a radiative plasmonic mode (extrinsic radiative channel), their optical spectrum carries an asymmetric line shape characteristic of Fano resonances.[14−17] Overall, subradiant modes have three different loss channels: Ohmic losses, the extrinsic coupling to radiation, and possibly their weak intrinsic dipole moment.[14−16,18] Among Fano-resonant systems, several designs have been proposed, such as dolmens,[18−20] nanocrosses,[21] plasmonic oligomers,[22−24] and ring-disk nanocavities.[13,25] Interactions with the substrate have also been used to tailor the near-field distribution for increased performances.[26,27] The high electromagnetic field enhancement generated from their excitation also serves as efficient platforms for surface-enhanced spectroscopy.[28,29] However, due to the complex nature of the optical spectrum associated with Fano-resonant systems, a general design method for highly sensitive plasmonic resonators with a low detection limit has not yet been formulated.

In this work, we investigate the performance of subradiant modes for refractive index sensing using a general analytical model and numerical calculations and address the specific features of Fano-resonant systems for refractive index sensing compared to Lorentz-resonant systems. We introduce a model predicting the impact that the different decay channels of subradiant modes have on the spectral resolution and contrast. We explicitly show that, by engineering their spectral dispersion, Fano-resonant systems have the potential to surpass Lorentzian plasmonic resonances for refractive index sensing: there exists an optimal value of the coupling for which the spectral dispersion is maximal and the reduction of Ohmic losses is the key to increasing this maximum in dispersion.

In particular, the sensitivity of subradiant modes with respect to global and local perturbations of the refractive index is first studied. A plasmonic nanostructure consisting of a dipolar nanoparticle on top of two parallel nanoparticles supporting a subradiant quadrupolar mode is considered, and the case of plasmonic heptamers is then used as an illustration. An explicit link between the sensitivity and the distribution of the mode field in the sensing region is shown. Using an analytical model, we show that both the line shape resolution and contrast determine the strength of the dispersion in Fano-resonant systems, and that Ohmic losses determine the line shape resolution and contrast. An expression for the intrinsic width of a plasmonic mode is derived and calculated with two methods: from the line shape parameters and using perturbation theory. Finally, a figure of merit for refractive index sensing with subradiant modes, given by the ratio of the sensitivity of the subradiant mode to its intrinsic width, is introduced. This figure of merit can be directly calculated from the line shape parameters in the far-field optical spectrum.

RESULTS AND DISCUSSION

Three Loss Channels in Fano-Resonant Systems. In this section, the different loss channels in Fano-resonant systems are defined. Figure 1a shows a plasmonic nanostructure with an optical response characterized by a Fano line shape.[20,29,30] The top metallic nanorod represented in red acts as an antenna for receiving and emitting light. It supports a plasmonic resonance with a Lorentzian line shape observable in the symmetric configuration (s = 0, Figure 1b). From Figure 1b, this mode has a dipolar distribution of charges. The resonance frequency ω_a of the dipolar mode is 1.60 eV in Figure 1, and its spectral width γ_a is 0.04 eV. On the other hand, the two bottom nanorods represented in

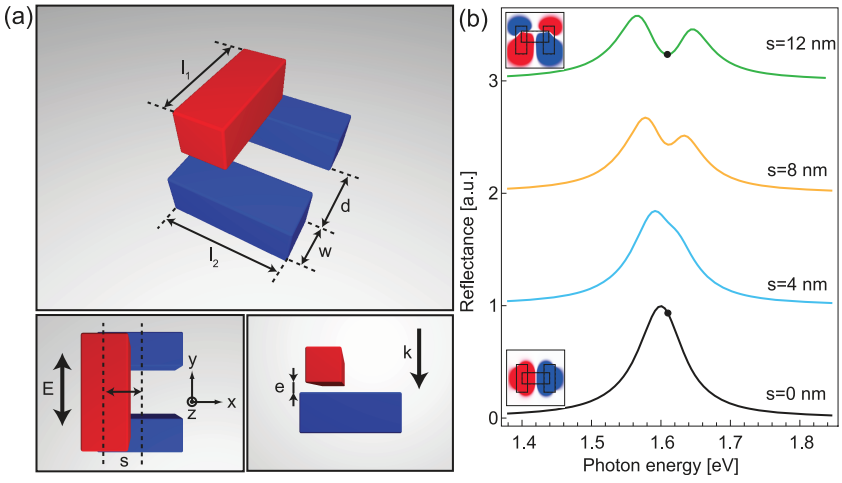

Figure 1. (a) Schematic of the geometry with $l_1 = l_2$ = 100 nm, w = 40 nm, d = 60, nm and e = 20 nm. The period along x and y direction is 500 nm. The refractive index of the surrounding environment is 1.33 (water), and the material of the nanoparticles is gold. (b) Reflectance spectra of the array for different values of the symmetry breaking s. Insets: Real part of the z-component of the instantaneous electric field on a (x,y) plane at half the distance between the top and bottom nanorods at a photon energy of 1.61 eV.

blue support a quadrupolar mode, whose electric field distribution is shown in Figure 1b. Its resonance frequency ω_0 is 1.61 eV. The coupling between the dipolar mode and the quadrupolar mode can be arbitrarily tuned by breaking the symmetry of the structure. In the symmetry-broken configuration, some energy is coupled from the dipolar mode to the quadrupolar mode; the energy stored in the quadrupolar mode is either decayed in the metallic nanostructures or coupled back to the dipolar mode.[29] The resonance width γ of the quadrupolar mode is given by the sum of two contributions: the intrinsic damping γ_i and an extrinsic radiative damping γ_c. The intrinsic damping γ_i is associated with the quadrupolar mode only, whereas the extrinsic radiative damping γ_c is related to its coupling to the dipolar mode. The dipolar mode's Lorentzian response R_a is modulated by this asymmetric line shape so that the total response R satisfies[31]

$$R = R_a \frac{(\omega - \omega_0 + q\gamma)^2 + b\gamma^2}{(\omega - \omega_0)^2 + \gamma^2} \quad (1)$$

where the parameters q and b describe the modulation asymmetry and damping, respectively. In Figure 1b, the reflectance spectra of the system for various values of the symmetry breaking are calculated numerically. In the symmetric configuration, the excitation of the subradiant mode is forbidden by symmetry, so that the response is only given by a Lorentzian. When the symmetry is broken, the mode coupling increases, resulting in an increase of the extrinsic contribution γ_c to the Fano resonance width. The modulation damping parameter can be written as the ratio of the intrinsic width γ_i to the total width γ:[29] $b = \gamma_i^2/(\gamma_c + \gamma_i)^2$. The asymmetry parameter provides the spectral location of the constructive and destructive interferences associated with the Fano line shape (Supporting Information of Gallinet *et al.*[29]): $q = (\omega_a^2 - \omega_0^2)/(2\gamma_a(1 + \gamma_i/\gamma_c))$.

In the example of Figure 1, the dipole moment of the quadrupolar mode vanishes so that only Ohmic losses contribute to the intrinsic damping γ_i. In general, a Fano resonance can still occur also when a weakly radiating mode (with a small but nonvanishing dipole moment) is coupled to a mode with a large dipole moment. The intrinsic damping γ_i has, in this case, both a nonradiative and a radiative contribution. In the following, the weakly radiating mode will be referred to as the subradiant mode.[13] The subradiant mode has therefore two different radiative loss channels, in addition to the nonradiative loss channel: one (intrinsic) from its dipole moment and the other (extrinsic) from its coupling to the radiative mode. These two channels contribute differently to the resonance line shape, in particular, to the modulation damping. In more complex systems, the extrinsic coupling can be divided in many different channels.[32] As will be discussed in the following, the control of these various loss channels is key to engineering Fano resonances with a sharp spectral dispersion.

Bulk and Local Sensitivity of Subradiant Modes. The first important aspect determining the performance of a plasmonic mode for refractive index sensing is its sensitivity. In this section, the sensitivity of Fano-resonant systems will be compared to the theoretical limit and to the sensitivity of Lorentz-resonant systems. The requirements for a figure of merit for Fano-resonant systems will be discussed.

Because of the small volume of plasmonic modes, a very small perturbation of the surrounding refractive index at the nanoscale induces a large shift of their resonance frequency. If the refractive index of the system is perturbed by an amount Δn within a volume V, the frequency ω_0 of the plasmon mode shifts by an amount $\Delta\omega$ given by

$$\Delta\omega \simeq -\Delta n \frac{\omega_0}{n} V_E \quad (2)$$

where n is the initial refractive index in the perturbation region V, and V_E is the fraction of electric field inside the volume V of perturbation. Equivalents of eq 2 have been derived using perturbation theory.[10,12] Its derivation is shown for completeness in the Methods section. Equation 2, which is valid for both radiative and subradiant modes, implies that the frequency shift of the mode is linear with respect to the refractive index perturbation. The frequency shift per unit of refractive index $\Delta\omega/\Delta n$ is the sensitivity of the mode. In Figure 2, the perturbation is applied to the entire environment, which can model, for example, a change in the composition of the liquid surrounding the nanoparticles. The refractive index of the unperturbed environment is chosen to be 1.33, corresponding to the refractive index of water. In this particular case of bulk perturbation, the spectral shift is determined by the proportion of the field that lies in the environment (as opposed to the field inside the metal). The maximal sensitivity that an electromagnetic mode can reach corresponds to the situation where the entire mode lies inside the perturbation region: $(\Delta\omega/\Delta n)_{max} \simeq -\omega_0/n$. The shift as a function of the refractive index perturbation for a symmetry breaking of 10 nm is reported in Figure 2a. The sensitivity is calculated by fitting a linear function and extracting the slope which gives $\Delta\omega/\Delta n = -0.91$ eV·RIU^{-1}. As expected, this value is below the maximal possible sensitivity of -1.21 eV·RIU^{-1}. From eq 2, the ratio of the sensitivity to the maximal sensitivity $(\Delta\omega/\Delta n)/(\Delta\omega/\Delta n)_{max}$ corresponds to the proportion of the electric field in the surrounding environment, which in this case is 76%. In order to increase the sensitivity, the electric field distribution of the subradiant mode can be engineered so that ideally 100% of the field lies in the sensing region. The best improvement in sensitivity $\Delta\omega/\Delta n$ that can be expected is only $(100 - 76)/76 \simeq 32\%$ in this case. This implies that both the antenna modes and

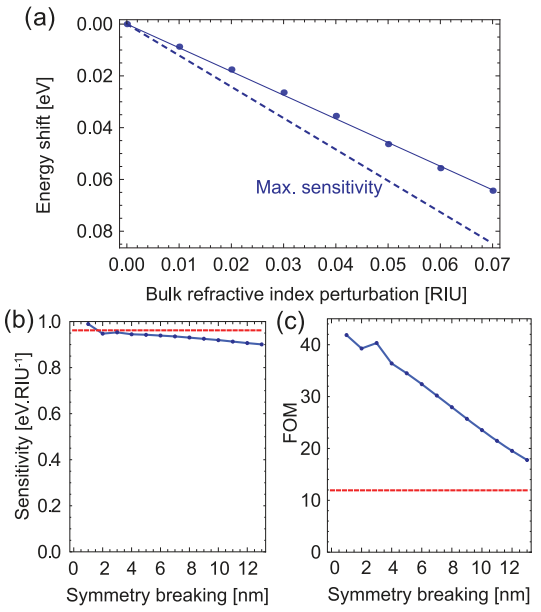

Figure 2. (a) Shift of the Fano resonance frequency as a function of the bulk refractive index perturbation. (b) Corresponding sensitivity as a function of the symmetry breaking *s*. The dashed red line represents the sensitivity of the Lorentzian plasmon resonance in the symmetric configuration. (c) Figure of merit (FOM) as a function of the symmetry breaking *s*. The dashed red line represents the FOM of the Lorentzian plasmon resonance in the symmetric configuration.

the subradiant modes have bulk sensitivities close to the theoretical limit. Experiments on highly sensitive subradiant modes have been reported in various plasmonic systems.[4,23]

Let us now consider a local perturbation of the refractive index. This situation models, for instance, the binding of a biochemical analyte to the nanoparticles surface[4,18,33] or the conformal coverage by a graphene sheet.[34] In this case, the sensitivity factor (eq 2) and the FOM (eq 3) strongly depend on the volume and location of the perturbation. The perturbation induces a significant spectral shift when it is placed in the region where the field is the most intense and can also be further enhanced if the resonance frequency is matched with the frequency of the vibrational states of the attached biomolecules.[4,18] Sensitive detection of molecular monolayers has been experimentally reported using a Fano-resonant system analogous to the geometry in Figure 1.[18] A possible experimental realization of local perturbation of the subradiant mode in a three-dimensional structure such as in Figure 1 would be the following: the fully covered single nanorod, a dielectric spacer, and the two parallel nanorods on top which are left uncovered and coated with a biomolecular monolayer. As an example in Figure 3, a layer of 4 nm and refractive index 1.55 is added around the nanoparticles surface. The respective shifts of the dipolar mode and the subradiant mode (not shown here) are also linear with respect to

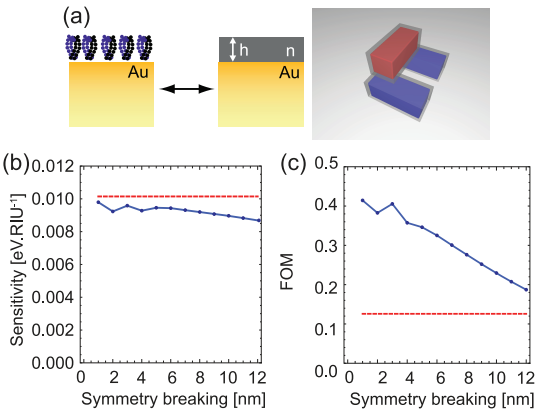

Figure 3. (a) Local refractive index perturbation (*i.e.*, by selective binding of biomolecules) is represented by an additional layer with a refractive index of 1.55 and a thickness of 4 nm around the nanostructure surface. (b) Corresponding sensitivity as a function of the symmetry breaking *s*. The dashed red line represents the sensitivity of the Lorentzian plasmon resonance in the symmetric configuration. (c) Corresponding figure of merit (FOM) as a function of the symmetry breaking *s*. The dashed red line represents the FOM of the Lorentzian plasmon resonance in the symmetric configuration.

the refractive index perturbation. As expected, the sensitivity is smaller than for the bulk refractive index sensing because the overlap between the perturbation volume and the field is smaller (Figure 3b). As the volume used for local sensing is included in the volume used for bulk sensing, a plasmonic mode which has a low performance for bulk sensing cannot be performing well for local sensing. From Figure 2b and Figure 3b, the sensitivities of Fano-resonant and Lorentz-resonant systems are in the same range. This implies, in particular, that the advantage of Fano-resonant systems as compared to Lorentz-resonant systems is not in their sensitivity but in their high spectral modulation, as will be discussed in the following.

The performance of a plasmonic mode for refractive index sensing also depends on the uncertainty in the determination of the resonance frequency.[12] An optical spectrum with sharp spectral features gives a low limit of detection, corresponding to the minimal perturbation that can be detected. For experimental and numerical approaches where the shift is calculated by fitting the entire line shape to an analytical formula, the accuracy and stability of this fit in determining the resonance frequency depend on the strength of the intensity variations of the line shape. In experimental measurements, the accuracy is determined by the signal-to-noise ratio, which also depends on the strength of the intensity variation at a fixed frequency. For plasmon resonance with a Lorentzian line shape, the spectral dispersion is directly related to the spectral width γ, so that a standard figure of merit (FOM) has been introduced as:[11]

$$\mathrm{FOM} = \frac{\text{sensitivity (eV}\cdot\text{RIU}^{-1})}{2\gamma\ \text{(eV)}} \qquad (3)$$

For Lorentz resonances, eq 3 can be interpreted in general as the product of the plasmonic mode's sensitivity with the local curvature of its spectral line shape (Methods). The FOM is a unitless number characterizing the performance of a plasmon resonance for refractive index sensing. Let us now evaluate the FOM for Lorentzian resonances in the case of Fano resonances, where the width γ of the Fano resonance can be obtained by locally fitting the spectrum to eq 1. The FOM of the Fano resonance as a function of the symmetry breaking is reported in Figure 2c and compared to the FOM of the Lorentzian resonance in the symmetric configuration. By definition, the FOM of the Fano resonance is larger because its line shape is spectrally narrower than the Lorentzian resonance. As the symmetry breaking increases, the Fano resonance width γ increases, and by definition, the FOM drastically drops from 41.8 to 17.8. The sensitivity of both modes is still comparable. The standard FOM (eq 3) defined originally for Lorentzian resonances considers only the spectral width as criterion for the limit of detection. However, in realistic Fano-resonant systems, a small spectral width is associated with a low modulation depth so that overall the spectral dispersion is weak (Figure 1). As a result, the uncertainty on the position of the Fano resonance frequency, which determines the limit of detection, remains high. This situation appears in Figure 2c and Figure 3c for low symmetry breaking: the sensitivity and FOM calculations converge in a slower way, and fluctuations are observed. Therefore, in Fano-resonant systems, the contrast of the modulation is also a very important quantity which determines the performance for refractive index sensing, together with the sensitivity and the spectral resolution. As the FOM only includes the sensitivity and the spectral resolution, a paradoxal situation is observed where the highest FOM is attributed to a Fano resonance with the weakest modulation. Therefore, the standard FOM as defined in eq 3 does not accurately characterize Fano-resonant systems.

Sensitivity, Spectral Resolution, and Contrast in a Figure of Merit. It has been previously highlighted that the performance of a Fano-resonant system for refractive index sensing depends on its sensitivity and the strength of the intensity variations of the line shape. The intensity variation is given by the first derivative of the line shape and has a maximum on the flanks. A direct method to evaluate the intensity variations on the flanks is to calculate the second derivative at the resonance frequency, which gives the curvature of the Fano line shape. In analogy, the second derivative of a Lorentzian line shape at its central frequency is proportional to its width (Methods). In a Fano-resonant system, this curvature vanishes for zero extrinsic coupling γ_c, as well as for large values of γ_c (Figure 1). In fact, the curvature as a function of the coupling can be calculated analytically from the line shape parameters and is proportional to $(1 - b)/\gamma^2$ in the symmetric case

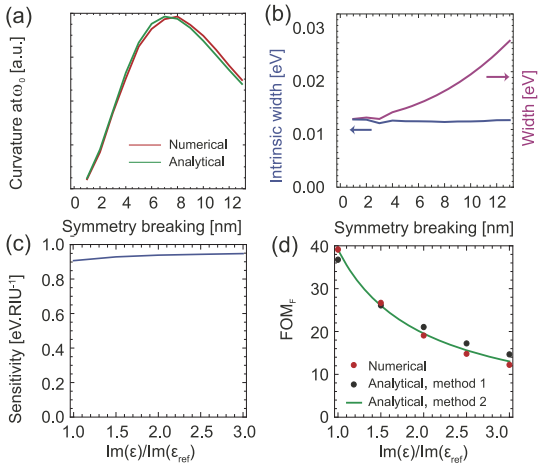

Figure 4. (a) Curvature (*i.e.*, second derivative) of the Fano line shape at the resonance frequency ω_0 as a function of the symmetry breaking. Red: computed numerically. Green: evaluated from the line shape parameters. (b) Purple: spectral width γ of the Fano resonance as a function of the symmetry breaking *s*. Blue: intrinsic width defined by $\gamma_i = \sqrt{b}\gamma$, as a function of the symmetry breaking *s*. (c) Bulk sensitivity as a function of the imaginary part of the metal permittivity ε compared to the reference value ε_{ref} for *s* = 12 nm. (d) FOM_F as a function of the imaginary part of the metal permittivity calculated with three different methods: from a fit of the sensitivity and the line shape parameters (red dots), using a fit of the sensitivity in panel (c) and eqs 2 and 4 (black dots), and using the linear dependence of the intrinsic width in the conductivity from the model of eq 4 (green curve).

(q = 0, Methods). In Figure 4a, the line shape parameters extracted from the fit are used to plot the curvature as a function of the symmetry breaking. The analytical formula is in perfect agreement with the numerically computed second derivative at the resonance frequency. The curvature reaches a maximum when $\gamma_c = (\sqrt{2} - 1)\gamma_i$, corresponding to $b = 1/2$. With this particular value of the coupling, the Fano line shape shows the largest spectral intensity variations and therefore is in the optimum configuration for refractive index sensing.

Let us now discuss how to obtain large spectral intensity variations with a Fano-resonant system. As the extrinsic coupling γ_c has to be adjusted to match the condition b = 1/2 for maximal curvature, the intrinsic width determines the value of this maximum, that is, the limit of detection that can be reached. The intrinsic width can be extracted from the far-field: it can be analytically shown that the product $\sqrt{b}\gamma = \gamma_i$ is independent of γ_c. In Figure 4b, this product is calculated numerically. As expected, it is constant and corresponds to the value of the Fano resonance width when the coupling of the modes approaches zero. In the absence of an intrinsic dipole moment, an analytical formula for the intrinsic width can be derived (Methods):

$$\gamma_i = \frac{\omega_0}{2}\left|\frac{\mathrm{Im}(\varepsilon_{metal})}{\mathrm{Re}(\varepsilon_{metal})}\right| v_C \qquad (4)$$

where ε_{metal} is the complex dielectric permittivity of the metallic structure and V_C is the fraction of modal field inside the volume C of conductive material. Equation 4 implies in particular that intrinsic losses depend on the conductivity of the material and the penetration of the field in the conductive material.

Let us now show that the value of the field penetration in eq 4 can be directly obtained from the sensitivity of the mode to bulk refractive index perturbations, without the need to compute the near-field explicitly. The sensitivity $\Delta\omega/\Delta n$ extracted from the fit in Figure 1a provides the relative amount of field in the surrounding environment from eq 2. In this geometry, the volume covered by the metal is complementary to the volume covered by the surrounding environment. As 76% of the field was found to lie in the environment, it can be considered that 24% of the field lies in the metallic volume. This value of the relative field penetration in the metallic structure can be directly inserted in eq 4. At a photon energy of 1.61 eV, the permittivity of the gold structure is equal to $\varepsilon_0(-21.75 + 1.35i)$ (according to Johnson and Christy[35]), which gives an instrinsic width of 0.0122 eV. This value is in very good agreement with the average value of 0.0115 eV of the product $\sqrt{b}\gamma$ in Figure 4b. This confirms that the intrinsic width of a plasmonic mode satisfies eq 4 and shows that it can be calculated using perturbation theory and without the need to perform field integrals. This method of calculation can be generalized to any volume and geometry: in order to calculate the relative amount of field in a volume V made of a homogeneous material, one can calculate the sensitivity of the mode with respect to a perturbation of the dielectric permittivity in the volume V and extract the relative amount of the field from the sensitivity. We have therefore shown two different methods to compute the intrinsic width of a subradiant mode: one from the resonance parameters and the other using perturbation theory. The intrinsic width γ_i, responsible for the spectral dispersion, can be engineered in two different ways: either on the conductive material to reduce the ratio $|\mathrm{Im}(\varepsilon_{metal})/\mathrm{Re}(\varepsilon_{metal})|$ or on the subradiant mode field distribution.

Overall, it appears that Ohmic losses and the sensitivity are the key elements for the design of an efficient refractive index sensor based on subradiant modes. The following figure of merit combines these two aspects in a unitless number:

$$\mathrm{FOM_F} = \frac{\text{sensitivity (eV}\cdot\text{RIU}^{-1})}{2\sqrt{b}\gamma\ \text{(eV)}} \qquad (5)$$

where the product $\sqrt{b}\gamma$ is equal to the intrinsic width of the subradiant mode and can be directly calculated from the far-field spectrum. The $\mathrm{FOM_F}$ is intrinsic to the subradiant mode and takes into account its sensitivity, the spectral resolution, and the contrast of the line shape. Compared to the definition of the standard FOM (eq 3), the factor $\sqrt{b}$ in eq 5 corrects for the fact that a narrow Fano line shape is also less modulated. The $\mathrm{FOM_F}$ with 8 nm symmetry breaking is 41.2 and 0.3 for bulk and local perturbation, respectively. The value of 8 nm for the symmetry breaking corresponds to the condition $b = 1/2$ for which the spectral modulation is maximized, but in some systems, the coupling is not always easily tunable and this particular regime cannot be reached.[31] In Figure 4c,d, the imaginary part of the nanoparticles' permittivity is multiplied by a factor of 1−3 as compared to the original value in Figure 2 in order to study the effect of the metal properties on the $\mathrm{FOM_F}$. The sensitivity of the subradiant mode remains generally constant because the modal field distribution is almost not affected by variations of the Ohmic losses. However, the intrinsic width increases drastically and, as a consequence, the $\mathrm{FOM_F}$ (Figure 4d). In Figure 4d, the $\mathrm{FOM_F}$ is calculated from the sensitivity using eq 2 and eq 4 (method 1), resulting in a very good agreement with respect to the values obtained by direct fitting of the sensitivity and the line shape parameters. The behavior of the $\mathrm{FOM_F}$ in Figure 4d can be predicted with a simple model (method 2), assuming that the sensitivity is constant and the intrinsic width is linear with Ohmic losses (eq 4). Such a strong dependence of the $\mathrm{FOM_F}$ (*i.e.*, the limit of detection) with respect to Ohmic losses motivates the optimization of conductive materials for plasmonic sensing applications.

Let us now apply this analysis to the case of plasmonic heptamers of two different materials (Figure 5), silver and gold. In this system, the outer ring of nanoparticles hybridizes with the central particle to form a super-radiant mode and a subradiant mode with large and low dipole moments, respectively.[22−24] The interaction between the super-radiant and the subradiant modes leads to a Fano interference. The resonance parameters of eq 1 are extracted from a fit of the entire line shape (Methods). First, in panels a and b of Figure 5, the asymmetry of the Fano resonance is affected by the perturbation. When the difference in sensitivity between the super-radiant mode and the subradiant mode is not negligible compared to the width of the super-radiant mode γ_a, the asymmetry parameter is nonzero. The super-radiant mode is less sensitive than the subradiant mode, and as a consequence, their detuning and the asymmetry are perturbed by the change of refractive index. More specifically in Figure 5b, the fit gives $q = 0.22$ for a refractive index of 1.33, whereas it gives $q = 0.17$ for a refractive index of 1.40. The spectral line shape is more symmetric in the perturbed system. The second main observation is that since the material chosen in Figure 5a is silver, the subradiant mode has low intrinsic losses and a relatively high $\mathrm{FOM_F}$ compared to gold in Figure 5b. In the heptamer system, the

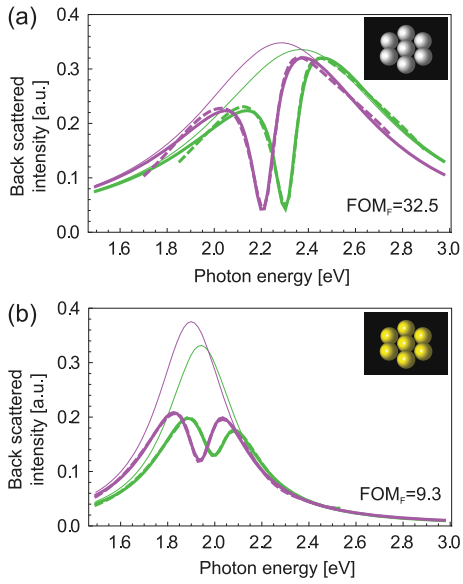

Figure 5. FOM$_F$ of an isolated (a) silver and (b) gold heptamer. The spheres' radius is 30 nm, and their center-to-center distance is 65 nm. The green and purple lines refer to a surrounding refractive index of 1.33 and 1.40, respectively. The thick solid line refers to the calculated back-scattered light intensity, the dashed line to the fit with the Fano resonance formula, and the thin solid line to the extracted Lorentzian envelope.

coupling between the subradiant mode and the super-radiant mode has not been tuned to match the condition of highest spectral dispersion (b = 1/2), but its FOM$_F$ can still be calculated and compared to the one of the system studied in Figure 1. A recent study also shows how the Fano line shape in such hybridized plasmonic systems can be precisely controlled, in particular, the modulation depth.[36] Comparing the obtained sensitivity to the maximal possible value shows that 80 and 60% of the electric field occupies the environment in the silver and gold heptamers, respectively (eq 2). This corresponds to a spectral width of 0.007 and 0.049 eV for the silver and gold heptamers, respectively. These values are smaller than their respective values of 0.021 and 0.059 eV for the intrinsic widths calculated from the product $\sqrt{b}\gamma$.

In the case of Figure 5, the heptamer is isolated and the subradiant mode can radiate to the side due to retardation effects.[37] In addition, its geometry is such that the total dipole moment of the subradiant mode is not vanishing. As a result, an intrinsic radiative loss channel is added to the subradiant mode, which contributes to the intrinsic width. In total, there are two radiative loss channels for the subradiant mode: one from its weak intrinsic dipole moment, and the other from its extrinsic coupling to the super-radiant mode. In such a nonideal case of interaction between two radiative modes, the calculation using eq 4 provides only the contribution from Ohmic losses to the intrinsic width of the subradiant mode, which means that the radiative and nonradiative contributions of the intrinsic width can be explicitly calculated using this method. The existence of a radiative channel intrinsic to the subradiant mode alters the spectral resolution and contrast for refractive index sensing, which emphasizes the importance of engineering its dipole moment (in Figure 1, the dipole moment of the quadrupolar mode is completely vanishing from symmetry). An additional radiative intrinsic loss channel can also be created when the subradiant mode is coupled to another bright mode, with an orthogonal polarization, for example.[38]

Finally, it has been seen that the control of the different loss channels in Fano-resonant systems is the key to a low limit of detection and to surpass Lorentz-resonant systems for refractive index sensing. This relies on a control of the electric field distribution in order to increase the sensitivity and decrease Ohmic losses. Such field engineering, together with the choice of conducting materials,[39] also paves the road to the optimal performance of a broad range of nano-optical devices such as plasmonic lasers,[40,41] waveguides,[42] surface-enhanced spectroscopy,[4,28] nonlinear devices,[43−45] molecular rulers,[29,46,47] and to the reduction of the power consumption of active nanoplasmonic devices and metamaterials.[48]

CONCLUSION

In summary, we have analyzed analytically and numerically the performance of subradiant modes for refractive index sensing. A nanosensor with a low limit of detection requires both a high sensitivity and a strong spectral dispersion of the resonance line shape. The sensitivity can be enhanced by concentrating the modal field to the sensing region, whereas the spectral dispersion is determined by Ohmic losses and the penetration of the field inside the conductive material. We have shown analytically and verified numerically that there exists an optimal value of the extrinsic coupling for which the spectral dispersion of the resonance line shape is maximal. The intrinsic width of the subradiant modes determines the value of the dispersion maximum. We have introduced a figure of merit given by the ratio of the sensitivity to the intrinsic width, which are both intrinsic properties of subradiant modes and fully characterize their efficiency for refractive index sensing. This figure of merit can be directly calculated from the line shape in the far-field optical spectrum and accounts for the fact that both the spectral resolution and contrast determine the limit of detection. An expression for the intrinsic width of a plasmonic mode has been derived and calculated with two methods: from the line shape parameters and using perturbation theory. Fano-resonant systems with low Ohmic losses have the potential to act as very efficient refractive index sensing platforms compared to Lorentz-resonant systems. This study paves the way

toward sensitive nanoscale biochemical sensors and immunoassays with a low limit of detection and, in general, any nano-optical device where Ohmic losses limit the performance.

METHODS

Numerical Calculations and Fits. The spectra have been calculated with a surface integral formulation.[49] The gold and silver permittivities of the nanoparticles are taken from experimental data.[35] A plane-wave illumination is always considered, and the ratio of the intensity of the scattered field to the intensity of the incident field yields the reflectance. The line shape parameters are calculated from fitting the reflectance spectra to eq 1. In the case of Figure 2 and Figure 3, the detuning between the dipolar and the quadrupolar modes is small as compared to the dipolar resonance width so that the modulation can be assumed to be symmetric ($q = 0$). The ratio of the total reflectance R to the reflectance in the symmetric system R_a is calculated and locally fitted by variation of the parameters γ and b. In the case of Figure 5, the two modes are supported by the same structure and the background reflectance R_a does not exist by itself. For each of the numerically calculated spectra, a fit by variation of seven parameters in eq 1 has been performed. For the Lorentzian response of the super-radiant mode R_a, these parameters are the central frequency ω_a, the spectral width γ_a, and the amplitude a. For the Fano modulation, the parameters considered are the central frequency ω_0, width γ, asymmetry q, and modulation damping b.

Spectral Dispersion of Lorentz and Fano Resonances. The line shape σ_L of Lorentz-resonant systems is given by the following function of the frequency: $\sigma_L(\omega) = \gamma_L^2/((\omega - \omega_L)^2 + \gamma_L^2)$. The dispersion is given by the first derivative σ_L', which vanishes at the resonance frequency ω_L and has a maximum on its flanks. The strength of the dispersion on the flanks is locally determined by the curvature (*i.e.*, the second derivative) at the resonance frequency. It can be easily shown that σ_L'' is proportionnal to $1/\gamma_L^2$, which means that the FOM in eq 3 is proportional to $\sqrt{\sigma_L''}$. As the spectral width γ_L increases, the FOM decreases monotonously. This behavior is in very good agreement with the decrease of the spectral resolution; therefore, the FOM is appropriate for Lorentz-resonant systems. For Fano-resonant systems, it is assumed for simplicity that their line shape is almost symmetric so that the parameter q is neglected. The line shape σ_F is given by $\sigma_F(\omega) = ((\omega - \omega_0)^2 + b\gamma^2)/((\omega - \omega_0)^2 + \gamma^2)$. The curvature of Fano-resonant systems is calculated in a similar way as for Lorentz-resonant systems: $\sigma_F''(\omega_0) = 2(1 - b)/\gamma^2$. The curvature is a non-monotonous function of the coupling γ_c, which has a maximum for $\gamma_c = (\sqrt{2} - 1)\gamma_i$, corresponding to $b = 1/2$. In this situation, the system possesses an optimal trade-off between spectral resolution and contrast. Ideally, a Fano-resonant system has therefore to be positioned in this coupling regime in order to optimize the strength of the spectral dispersion. In the expression of the FOM_F in eq 5, a factor $\sqrt{b}$ is introduced as a correction for the FOM including the contrast. It is proportionnal to the mode sensitivity and the last loss channel which needs to be engineered: Ohmic losses.

Sensitivity of a Localized Plasmon Mode. Let us consider the Feshbach decomposition of a electric field wave function $|\mathbf{E}\rangle$ into a radiative and a nonradiative parts:[16,50] $|\mathbf{E}\rangle = \underline{\underline{P}}|\mathbf{E}\rangle + \underline{\underline{Q}}|\mathbf{E}\rangle$. A unique nonradiative mode $\mathbf{E}_0$, defined as the eigenfunction of the projector to nonradiative modes, $\underline{\underline{Q}}|\mathbf{E}_0\rangle = |\mathbf{E}_0\rangle$, satisfies the following eigenvalue equation:[16]

$$(\underline{\underline{Q}}\,\underline{\underline{\mathscr{M}}}\,\underline{\underline{Q}} - \omega_0^2\,\underline{\underline{I}})|\mathbf{E}_0\rangle = 0 \qquad (6)$$

where ω_0 the real frequency eigenvalue associated to the nonradiative mode and $\underline{\underline{\mathscr{M}}}$ is a hermitian operator associated with the electric field wave equation:

$$\underline{\underline{\mathscr{M}}}\,\mathbf{E}(\mathbf{r}) = \frac{c_0^2}{\varepsilon(\mathbf{r})}\nabla \times \nabla \times \mathbf{E}(\mathbf{r}) \qquad (7)$$

The scalar product is defined by $\langle \mathbf{E}_1|\mathbf{E}_2\rangle = \int d^3\mathbf{r}\varepsilon(\mathbf{r})\mathbf{E}_1^*(\mathbf{r})\cdot\mathbf{E}_2(\mathbf{r})$ to guarantee the hermiticity of the operator $\underline{\underline{\mathscr{M}}}$. The nonradiative mode is normalized: $|\langle E_0|E_0\rangle|^2 = 1$. A perturbation of the dielectric permittivity $\Delta\varepsilon$ over a volume V is now assumed. Using perturbation theory, the shift $\Delta\omega$ of the frequency of the mode is given by[10,12]

$$\Delta\omega \simeq -\frac{\Delta n}{n}\,\omega_0\langle \mathbf{E}_0|\mathbf{E}_0\rangle_V \qquad (8)$$

where the scalar product of the field is restricted to the volume V of perturbation. Equation 8 is equivalent to eq 2.

Losses of a Localized Plasmon Mode. In the presence of a current field $|\mathbf{J}\rangle$, such as found in conductive materials, eq 6 can be written as

$$(\underline{\underline{Q}}\,\underline{\underline{\mathscr{M}}}\,\underline{\underline{Q}} - \omega_0^2\,\underline{\underline{I}})|\mathbf{E}\rangle = \frac{i\omega\mu c^2}{\varepsilon}\underline{\underline{Q}}|\mathbf{J}\rangle \qquad (9)$$

where μ is the relative magnetic permeability. The formal solution of eq 9 has the form of $|\mathbf{E}\rangle = |\mathbf{E}_0\rangle + (i\omega\mu c^2/\varepsilon)\underline{\underline{G}}_0\underline{\underline{Q}}|\mathbf{J}\rangle$, where $|\mathbf{E}_0\rangle$ is the solution of the homogeneous problem and $\underline{\underline{G}}_0$ its Green's dyadic function. Using a procedure equivalent to the one in a previous work (Supporting Information in Gallinet *et al.*[29]), the electric field wave function can be written as

$$\underline{\underline{Q}}\,\underline{\underline{\mathscr{M}}}\,\underline{\underline{Q}}|\mathbf{E}\rangle = \omega_0^2|\mathbf{E}_0\rangle \pm \frac{ic^2\mu\omega}{2\varepsilon}\langle \mathbf{E}_0|\mathbf{J}\rangle|\mathbf{E}_0\rangle \qquad (10)$$

where the sign of the second term is chosen with respect to causality. Let us now assume that the current field is governed by Ohm's law ($|\mathbf{J}\rangle = \sigma|\mathbf{E}\rangle$ with σ the conductivity of the material) and restricted to a region C corresponding to the presence of a conductive material. Equation 10 becomes in the assumption of low current:

$$\underline{\underline{Q}}\,\underline{\underline{\mathscr{M}}}\,\underline{\underline{Q}}|\mathbf{E}\rangle \simeq \left(\omega_0 \pm i\,\frac{\omega_0 \mathrm{Im}(\varepsilon)}{2\mathrm{Re}(\varepsilon)}\langle \mathbf{E}_0|\mathbf{E}_0\rangle_C\right)^2|\mathbf{E}\rangle \qquad (11)$$

where the scalar product of the field is restricted to the volume C of conductive material. Extracting the imaginary part of the eigenvalue in eq 11 yields eq 4.

Conflict of Interest: The authors declare no competing financial interest.

Acknowledgment. Funding from CCMX-FanoSense is gratefully acknowledged, as well as stimulating discussions with H. Giessen on experimental realizations of the three-dimensional structure of Figure 1 and Figure 3.

REFERENCES AND NOTES

1. Genet, C.; Ebbesen, T. W. Light in Tiny Holes. *Nature* **2007**, *445*, 39–46.
2. Maier, S. A. *Plasmonics: Fundamentals and Applications*; Springer Science: Berlin, 2007.
3. Anker, J. N.; Hall, W. P.; Lyandres, O.; Shah, N. C.; Zhao, J.; Van Duyne, R. P. Biosensing with Plasmonic Nanosensors. *Nat. Mater.* **2008**, *7*, 442–453.
4. Halas, N. J.; Lal, S.; Chang, W.-S.; Link, S.; Nordlander, P. Plasmons in Strongly Coupled Metallic Nanostructures. *Chem. Rev.* **2011**, *111*, 3913–3961.
5. Yan, B.; Boriskina, S. V.; Reinhard, B. M. Design and Implementation of Noble Metal Nanoparticle Cluster Arrays for Plasmon Enhanced Biosensing. *J. Phys. Chem. C* **2011**, *115*, 24437–24453.

6. Zhang, W.; Fischer, H.; Schmid, T.; Zenobi, R.; Martin, O. J. F. Mode-Selective Surface-Enhanced Raman Spectroscopy Using Nanofabricated Plasmonic Dipole Antennas. *J. Phys. Chem. C* **2009**, *113*, 14672–14675.
7. Juan, M. L.; Righini, M.; Quidant, R. Plasmon Nano-Optical Tweezers. *Nat. Photonics* **2011**, *5*, 349–356.
8. Langhammer, C.; Larsson, E. M.; Kasemo, B.; Zoric, I. Indirect Nanoplasmonic Sensing: Ultrasensitive Experimental Platform for Nanomaterials Science and Optical Nanocalorimetry. *Nano Lett.* **2010**, *10*, 3529–3538.
9. Wang, S.; Ota, S.; Guo, B.; Ryu, J.; Rhodes, C.; Xiong, Y.; Kalim, S.; Zeng, L.; Chen, Y.; Teitell, M. A.; *et al.* Subcellular Resolution Mapping of Endogenous Cytokine Secretion by Nano-Plasmonic-Resonator Sensor Array. *Nano Lett.* **2011**, *11*, 3431–3434.
10. Joannopoulos, J. D.; Johnson, S. G.; Winn, J. N.; Meade, R. D. *Photonic Crystals: Molding the Flow of Light*, 2nd ed; Princeton University Press: Princeton, NJ, 2008.
11. Sherry, L.; Chang, S.; Schatz, G.; Van Duyne, R.; Wiley, B.; Xia, Y. Localized Surface Plasmon Resonance Spectroscopy of Single Silver Nanocubes. *Nano Lett.* **2005**, *5*, 2034–2038.
12. Unger, A.; Kreiter, M. Analyzing the Performance of Plasmonic Resonators for Dielectric Sensing. *J. Phys. Chem. C* **2009**, *113*, 12243–12251.
13. Hao, F.; Nordlander, P.; Sonnefraud, Y.; Van Dorpe, P.; Maier, S. A. Tunability of Subradiant Dipolar and Fano-Type Plasmon Resonances in Metallic Ring/Disk Cavities: Implications for Nanoscale Optical Sensing. *ACS Nano* **2009**, *3*, 643–652.
14. Luk'yanchuk, B.; Zheludev, N. I.; Maier, S. A.; Halas, N. J.; Nordlander, P.; Giessen, H.; Chong, C. T. The Fano Resonance in Plasmonic Nanostructures and Metamaterials. *Nat. Mater.* **2010**, *9*, 707–715.
15. Miroshnichenko, A. E.; Flach, S.; Kivshar, Y. S. Fano Resonances in Nanoscale Structures. *Rev. Mod. Phys.* **2010**, *82*, 2257–2298.
16. Gallinet, B.; Martin, O. J. F. *Ab Initio* Theory of Fano Resonances in Plasmonic Nanostructures and Metamaterials. *Phys. Rev. B* **2011**, *83*, 235427.
17. Giannini, V.; Francescato, Y.; Amrania, H.; Phillips, C. C.; Maier, S. A. Fano Resonances in Nanoscale Plasmonic Systems: A Parameter-Free Modeling Approach. *Nano Lett.* **2011**, *11*, 2835–2840.
18. Wu, C.; Khanikaev, A. B.; Adato, R.; Arju, N.; Yanik, A. A.; Altug, H.; Shvets, G. Fano-Resonant Asymmetric Metamaterials for Ultrasensitive Spectroscopy and Identification of Molecular Monolayers. *Nat. Mater.* **2012**, *11*, 69–75.
19. Verellen, N.; Sonnefraud, Y.; Sobhani, H.; Hao, F.; Moshchalkov, V. V.; Van Dorpe, P.; Nordlander, P.; Maier, S. A. Fano Resonances in Individual Coherent Plasmonic Nanocavities. *Nano Lett.* **2009**, *9*, 1663–1667.
20. Liu, N.; Weiss, T.; Mesch, M.; Langguth, L.; Eigenthaler, U.; Hirscher, M.; Soennichsen, C.; Giessen, H. Planar Metamaterial Analogue of Electromagnetically Induced Transparency for Plasmonic Sensing. *Nano Lett.* **2010**, *10*, 1103–1107.
21. Verellen, N.; Van Dorpe, P.; Huang, C.; Lodewijks, K.; Vandenbosch, G. A. E.; Lagae, L.; Moshchalkov, V. V. Plasmon Line Shaping Using Nanocrosses for High Sensitivity Localized Surface Plasmon Resonance Sensing. *Nano Lett.* **2011**, *11*, 391–397.
22. Fan, J. A.; Wu, C.; Bao, K.; Bao, J.; Bardhan, R.; Halas, N. J.; Manoharan, V. N.; Nordlander, P.; Shvets, G.; Capasso, F. Self-Assembled Plasmonic Nanoparticle Clusters. *Science* **2010**, *328*, 1135–1138.
23. Lassiter, J. B.; Sobhani, H.; Fan, J. A.; Kundu, J.; Capasso, F.; Nordlander, P.; Halas, N. J. Fano Resonances in Plasmonic Nanoclusters: Geometrical and Chemical Tunability. *Nano Lett.* **2010**, *10*, 3184–3189.
24. Hentschel, M.; Dregely, D.; Vogelgesang, R.; Giessen, H.; Liu, N. Plasmonic Oligomers: The Role of Individual Particles in Collective Behavior. *ACS Nano* **2011**, *5*, 2042–2050.
25. Fu, Y. H.; Zhang, J. B.; Yu, Y. F.; Luk'yanchuk, B. Generating and Manipulating Higher Order Fano Resonances in Dual-Disk Ring Plasmonic Nanostructures. *ACS Nano* **2012**, *6*, 5130–5137.
26. Zhang, S.; Bao, K.; Halas, N. J.; Xu, H.; Nordlander, P. Substrate-Induced Fano Resonances of a Plasmonic Nanocube: A Route to Increased-Sensitivity Localized Surface Plasmon Resonance Sensors Revealed. *Nano Lett.* **2011**, *11*, 1657–1663.
27. Cetin, A. E.; Altug, H. Fano Resonant Ring/Disk Plasmonic Nanocavities on Conducting Substrates for Advanced Biosensing. *ACS Nano* **2012**, *6*, 9989–9995.
28. Ye, J.; Wen, F.; Sobhani, H.; Lassiter, J. B.; Dorpe, P. V.; Nordlander, P.; Halas, N. J. Plasmonic Nanoclusters: Near Field Properties of the Fano Resonance Interrogated with SERS. *Nano Lett.* **2012**, *12*, 1660–1667.
29. Gallinet, B.; Siegfried, T.; Sigg, H.; Nordlander, P.; Martin, O. J. F. Plasmonic Radiance: Probing Structure at the Angstrom Scale with Visible Light. *Nano Lett.* **2013**, *13*, 497–503.
30. Taubert, R.; Hentschel, M.; Kästel, J.; Giessen, H. Classical Analog of Electromagnetically Induced Absorption in Plasmonics. *Nano Lett.* **2012**, *12*, 1367–1371.
31. Gallinet, B.; Martin, O. J. F. Influence of Electromagnetic Interactions on the Line Shape of Plasmonic Fano Resonances. *ACS Nano* **2011**, *5*, 8999–9008.
32. Yoon, J.; Seol, K. H.; Song, S. H.; Magnusson, R. Critical Coupling in Dissipative Surface-Plasmon Resonators with Multiple Ports. *Opt. Express* **2010**, *18*, 25702–25711.
33. Piliarik, M.; Kvasnicka, P.; Galler, N.; Krenn, J. R.; Homola, J. Local Refractive Index Sensitivity of Plasmonic Nanoparticles. *Opt. Express* **2011**, *19*, 9213–9220.
34. Mousavi, S. H.; Kholmanov, I.; Alici, K. B.; Purtseladze, D.; Arju, N.; Tatar, K.; Fozdar, D. Y.; Suk, J. W.; Hao, Y.; Khanikaev, A. B.; *et al.* Inductive Tuning of Fano-Resonant Metasurfaces Using Plasmonic Response of Graphene in the Mid-Infrared. *Nano Lett.* **2013**, *13*, 1111–1117.
35. Johnson, P. B.; Christy, R. W. Optical-Constants of Noble-Metals. *Phys. Rev. B* **1972**, *6*, 4370.
36. Lovera, A.; Gallinet, B.; Nordlander, P.; Martin, O. J. Mechanisms of Fano Resonances in Coupled Plasmonic Systems. *ACS Nano* **2013**, *7*, 4527–4536.
37. Gallinet, B.; Martin, O. J. F. The Relation between Near-Field and Far-Field Properties of Plasmonic Fano Resonances. *Opt. Express* **2011**, *19*, 22167–22175.
38. Wu, C.; Khanikaev, A. B.; Shvets, G. Broadband Slow Light Metamaterial Based on a Double-Continuum Fano Resonance. *Phys. Rev. Lett.* **2011**, *106*, 107403.
39. Tassin, P.; Koschny, T.; Kafesaki, M.; Soukoulis, C. M. A Comparison of Graphene, Superconductors and Metals as Conductors for Metamaterials and Plasmonics. *Nat. Photonics* **2012**, *6*, 259–264.
40. Zheludev, N. I.; Prosvirnin, S. L.; Papasimakis, N.; Fedotov, V. A. Lasing Spaser. *Nat. Photonics* **2008**, *2*, 351–354.
41. Ma, R.-M.; Oulton, R. F.; Sorger, V. J.; Bartal, G.; Zhang, X. Room-Temperature Sub-Diffraction-Limited Plasmon Laser by Total Internal Reflection. *Nat. Mater.* **2011**, *10*, 110–113.
42. Bergman, D. J.; Stockman, M. I. Surface Plasmon Amplification by Stimulated Emission of Radiation: Quantum Generation of Coherent Surface Plasmons in Nanosystems. *Phys. Rev. Lett.* **2003**, *90*, 027402.
43. Tuovinen, H.; Kauranen, M.; Jefimovs, K.; Vahimaa, P.; Vallius, T.; Turunen, J.; Tkachenko, N. V.; Lemmetyinen, H. Linear and Second-Order Nonlinear Optical Properties of Arrays of Noncentrosymmetric Gold Nanoparticles. *J. Nonlinear Opt. Phys. Mater.* **2002**, *11*, 421–432.
44. Zhang, Y.; Grady, N. K.; Ayala-Orozco, C.; Halas, N. J. Three-Dimensional Nanostructures as Highly Efficient Generators of Second Harmonic Light. *Nano Lett.* **2011**, *11*, 5519–5523.
45. Thyagarajan, K.; Butet, J.; Martin, O. J. F. Augmenting Second Harmonic Generation Using Fano Resonances in Plasmonic Systems. *Nano Lett.* **2013**, *13*, 1847–1851.
46. Sonnichsen, C.; Reinhard, B. M.; Liphardt, J.; Alivisatos, A. P. A Molecular Ruler Based on Plasmon Coupling of Single Gold and Silver Nanoparticles. *Nat. Biotechnol.* **2005**, *23*, 741–745.

47. Liu, N.; Hentschel, M.; Weiss, T.; Alivisatos, A. P.; Giessen, H. Three-Dimensional Plasmon Rulers. *Science* **2011**, *332*, 1407–1410.
48. Hess, O.; Pendry, J. B.; Maier, S. A.; Oulton, R. F.; Hamm, J. M.; Tsakmakidis, K. L. Active Nanoplasmonic Metamaterials. *Nat. Mater.* **2012**, *11*, 573–584.
49. Gallinet, B.; Martin, O. J. F. Scattering on Plasmonic Nanostructures Arrays Modeled with a Surface Integral Formulation. *Photonic Nanostruct.* **2010**, *8*, 278–284.
50. Feshbach, H. A Unified Theory of Nuclear Reactions 0.2. *Ann. Phys.* **1962**, *19*, 287–313.